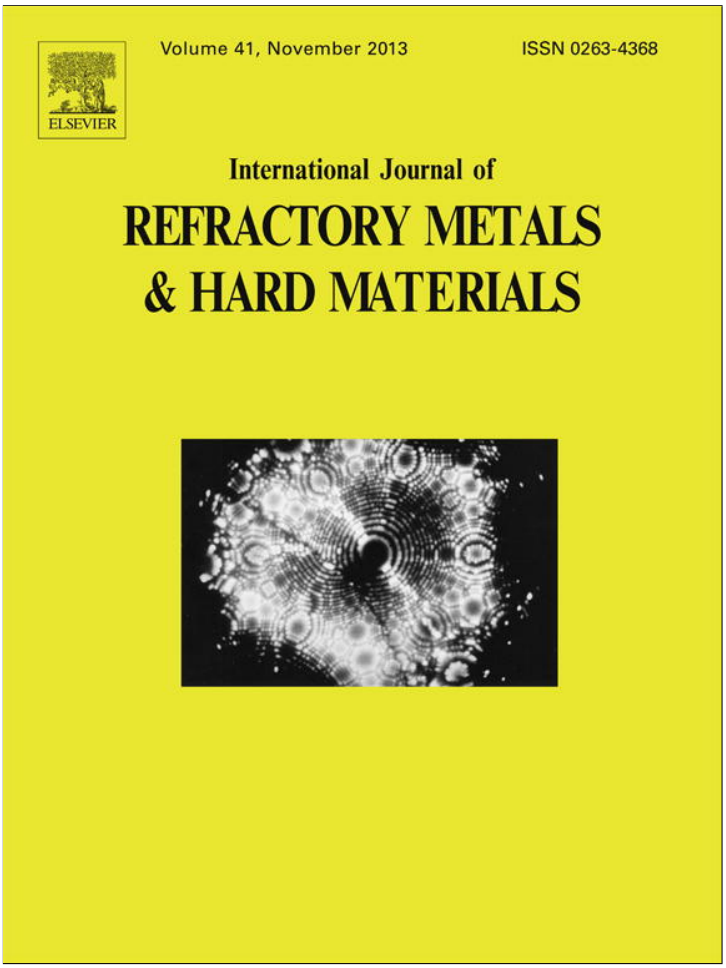

Int. Journal of Refractory Metals and Hard Materials 41 (2013) 198–209

Contents lists available at ScienceDirect

Int. Journal of Refractory Metals and Hard Materials

journal homepage: www.elsevier.com/locate/IJRMHM

Influence of wire-EDM on high temperature sliding wear behavior of WC10Co(Cr/V) cemented carbide

Y. Pérez Delgado [a], P. De Baets [a], K. Bonny [a], V. Carretero Olalla [b], J. Vleugels [c], B. Lawers [d], M.H. Staia [a,*]

[a] Ghent University, Mechanical Construction and Production Department, Technologiepark 903, Zwijnaarde, B-9052, Gent, Belgium
[b] Ghent University, Department of Materials Science and Engineering, Technologiepark 903, Zwijnaarde, B-9052, Gent, Belgium
[c] Catholic University of Leuven (K.U. Leuven), Metallurgy and Materials Engineering Department, Kasteelpark Arenberg 44, BE-3001, Leuven, Belgium
[d] Catholic University of Leuven (K.U. Leuven), Mechanical Engineering Department, Celestijnenlaan 300 B, BE-3001, Leuven, Belgium

ARTICLE INFO

Article history:
Received 19 January 2013
Accepted 28 March 2013

Keywords:
Sliding wear
Wire EDM cemented carbide
High temperature wear
Friction coefficients
Wear mechanisms
Sliding contact
Residual stresses

ABSTRACT

This paper reports the friction and wear response of WC–10%Co(Cr/V) cemented carbide with different surface finishes, attained by grinding (G) and wire-EDM, respectively, during sliding experiments at 400 °C. For comparison, tests under the same conditions were carried out at 25 °C. The wear experiments were performed under a normal force of 14 N, which produced a Hertzian maximum pressure of 3.10 GPa, and a sliding speed of 0.3 m/s against WC–6%Co(Cr/V) balls of 6 mm diameter. At 25 °C the average values of the friction coefficients were 0.36 ± 0.04 and 0.39 ± 0.06 for the ground and wire-EDM surface finishes, respectively. The mechanical behavior of both systems at 25 °C was assessed by carrying out analytical calculations of the stress field created by a circular sliding contact under a spherical indenter, where the residual stresses were considered. The theoretical results are in agreement with the experimental data, indicating that the wire-EDM sample has a specific wear rate, which is approximately 3.1 times greater than that corresponding to the G sample at 25 °C. At 400 °C, an increase in the friction coefficients takes place up to values of 0.75 ± 0.1 and 0.71 ± 0.8, for the ground and wire-EDM surface finishes, respectively. The increase was associated to an adhesive mechanism, which is more pronounced for the G sample. However, for the wire-EDM sample this increase was more linked to a marked abrasive mechanism. The wear rates for both samples at 400 °C are similar to those obtained at 25 °C, which indicates that apparently the test temperature does not have an important effect on the wear rate. However, it is known that temperature influences considerably the residual stress nature. Therefore, these results were explained by taking into account the wear mechanisms between the tribopairs in view of the mechanical characteristics and the morphological features obtained from SEM coupled with EDS analysis.

1. Introduction

In the last three decades, the EMD process has been one of the most important abrasion-less machining methods for hard and brittle materials, which employs a series of electrical sparks to erode the superfluous work-material and to generate the desired shape. The feasibility of implementing EDM for conforming cemented carbides has been successfully proven and, more specifically, this method is considered to be an efficient technology to machine WC–Co cemented carbides [1–5]. However, a disadvantage of EDM is that it induces a heat-affected zone (HAZ) including micro-cracks, craters and unfavorable stresses just beneath the shaped surface [6,7]. Consequently, the defects on the machined surface severely reduce the service life, reliability and machining precision of a tool or a mould made of WC-based alloys.

Therefore, detailed information on the influence of EDM on mechanical or tribological properties of cemented carbides is essential if the performance reliability associated with the structural application of EDM'ed cemented carbides is to be improved.

In the literature, an important amount of research has been published regarding the influence of the HAZ on different aspects related to the behavior of cemented carbides, such as surface integrity [8,9], surface roughness [10], flexural strength [11–13], fracture and fatigue resistance [8], as well as hardness [14].

With respect to the impact of wire-EDM machining process on friction and wear, extensive research was carried out under reciprocating sliding motion mode on a number of commercial WC–Co cemented carbides with 6–12%Co and different additions of grain refiners [15–21]. It has been shown that the grain size distribution and cobalt concentration are the major factors affecting the material removal rate and the attainable surface smoothness. For example, by carrying out several consecutive EDM surface finishing steps, it

* Corresponding author at: School of Metallurgy and Materials Science, Faculty of Engineering, Universidad Central de Venezuela, Apartado 49141, Caracas 1040, Venezuela. Tel.: +58 2126051492.
E-mail addresses: mariana.staia@ucv.ve, mhstaia@gmail.com (M.H. Staia).

0263-4368/$ – see front matter © 2013 Elsevier Ltd. All rights reserved.
http://dx.doi.org/10.1016/j.ijrmhm.2013.03.013

allowed the average surface roughness to be reduced below Rt = 1.3 μm or Ra = 0.3 μm.

However, to the knowledge of the authors, there is a scarce information on the influence of wire-EDM on the friction response of cemented carbides under continuous sliding contact at high temperatures, although some reports on the wear response of WC–Co hard metals up to 600 °C have been recently published in the literature, using either alumina [22] or the same type of material [23] as counterpart.

Consequently, this paper aims to investigate the friction response of WC–Co/WC–Co cemented carbide tribopairs with different surface finishes attained by grinding and wire-EDM, respectively, during sliding experiments at 400 °C. For comparison, tests under the same conditions are carried out at room temperature. The test temperature of only 400 °C was selected to avoid significant effects of oxidation for WC–10%Co, since it was shown recently by Shi et al. [24] that the carbide starts to oxidize at about 425 °C and, at a temperature of 450 °C, an oxidation layer thickness of ~39 μm is already achieved, which is composed of oxides such as WO_3, Co_3O_4 and $CoWO_4$ phases, irrespective of the tested temperature.

2. Experimental

2.1. Test material

The present investigation has been conducted on a cemented carbide based material with 10%Co as metallic binder and with small amounts of Cr_3C_2 and VC, added as grain size inhibitors during sintering. The cemented carbide grades correspond to CERATIZIT grades of MG18 (WC10Co(Cr/V)) and this composition was chosen as result of our previous study [25] that indicated that this material has exhibited the best reciprocating wear and friction performance when compared with WC–10%Co without any additions.

The chemical, physical, mechanical and microstructural characteristics of the WC10Co(Cr/V) alloy, as well as the WC6Co(Cr/V) counter pin material are provided in Table 1.

The morphological characteristics of both carbides WC10Co(Cr/V) and WC6Co(Cr/V) grade samples are presented in the SEM micrographs in Fig. 1. As it can be observed, the WC10Co(Cr/V) grade has a finer microstructure, with an average grain size of 0.3 μm.

Plate specimens of WC10Co(Cr/V) alloys were machined and surface finished by both grinding and wire-EDM, respectively with final dimensions of 38 × 58 × 4 mm^3. The grinding and operation was conducted using a JF415DS grinding equipment (Jung, Göppingen, Germany) by means of a diamond abrasive wheel (type MD4075B55, Wendt Boart, Brussels, Belgium) with a wheel diameter of 200 mm, average abrasive grain size of 54 μm, wheel speed of 22 m/s, table speed of 12 m/min and cutting depth of 10 μm.

Wire electrical plate charge machining (wire-EDM) was performed on a ROBOFIL 2030SI technology (Charmilles Technologies, Switzerland)

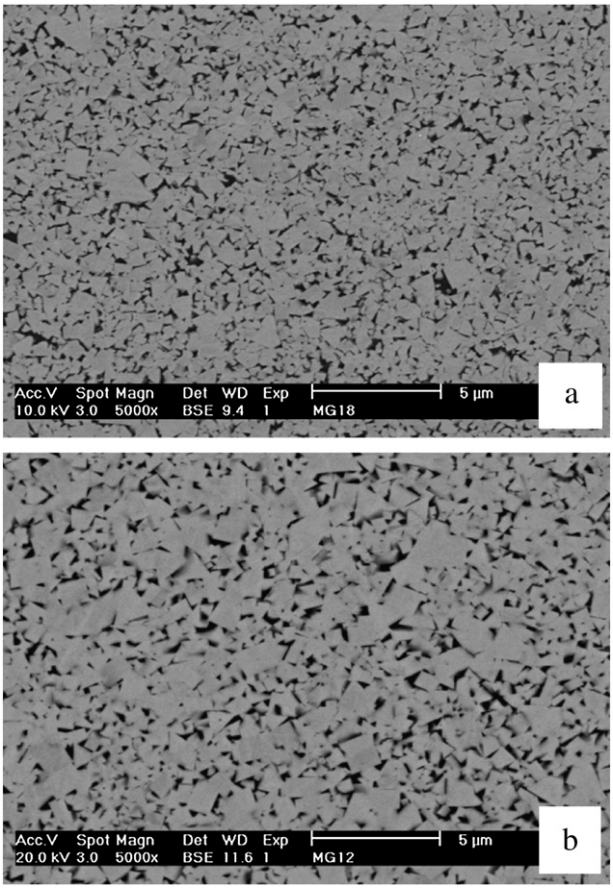

Fig. 1. SEM images in BSE mode revealing the microstructure of (a) WC10Co(Cr/V) and (b) WC6Co(Cr/V); the bright phase corresponds to WC, and the dark phase corresponds to the binder.

in de-ionized water with dielectric conductivity of 5 μS/cm. The wire electrode consisted of a CuZn37 brass alloy with a diameter of 0.25 mm. Its tensile strength is of approximately 500 MPa. The wire-EDM machining route consisted of a rough material-removing step followed by 7 finishing steps. The first EDM step was carried out with high spark thermal energy in order to acquire high material removal rates. Subsequently, several finish steps with globally decreasing energy input and pulse duration were applied. Each consecutive EDM step cuts off the previous wire-EDM'ed surface with the goal to achieve a decreasing surface roughness and a higher surface quality.

The current research was focused on samples manufactured by means of the wire-EDM (E21), according to the optimum parameters already determined [15] for this material, shown in Table 2, which produced a recast layer of ~5 μm and a HAZ extension of ~12 μm, including the recast layer. The surface finish after grinding is regarded

Table 1
Properties for the cemented carbide based materials used as test samples[(a)] (plate) and the static counterpart[(b)] (pin).

Material properties	WC10Co(Cr/V)[(a)]	WC6Co(Cr/V)[(b)]
Grain growth inhibitor [wt.%]	0.8% Cr_3C_2/VC	0.8% Cr_3C_2/VC
Electrical resistivity [Ω.m]	1.7×10^{-7}	1.4×10^{-7}
HV_{10} [kg/mm^2]	1685 ± 4	1913 ± 1
HV_{30} [kg/mm^2]	1652 ± 5	1715 ± 4
K_{IC} (10 kg) [MPa.m$^{1/2}$]	11.0 ± 0.6	8.4 ± 0.2
K_{IC} (30 kg) [MPa.m$^{1/2}$]	9.7 ± 0.2	8.8 ± 0.2
Compressive strength [GPa]	6.6	7.2
Poisson constant	0.29	0.29
E-modulus [GPa]	541 ± 4	609 ± 4
Average WC grain size [μm]	0.32	0.55
d_{50} grain size [μm]	0.3	0.5
d_{90} grain size [μm]	0.6	1.0
d_{av} grain size [μm]	0.3	0.6

Table 2
Parameters for the machining of the E21 sample.

Wire-EDM regime	E21
Open voltage [V]	140
Pulse duration, t_e [μs]	1
Pulse interval, t_o [μs]	4
Maximum speed [mm/min]	6.1
Reference servo voltage, Aj [v]	6
Pulse ignition height, IAL [A]	4.5
Flushing pressure [bar]	0
Wire tension [N]	10
Wire winding speed [m/min]	6.8

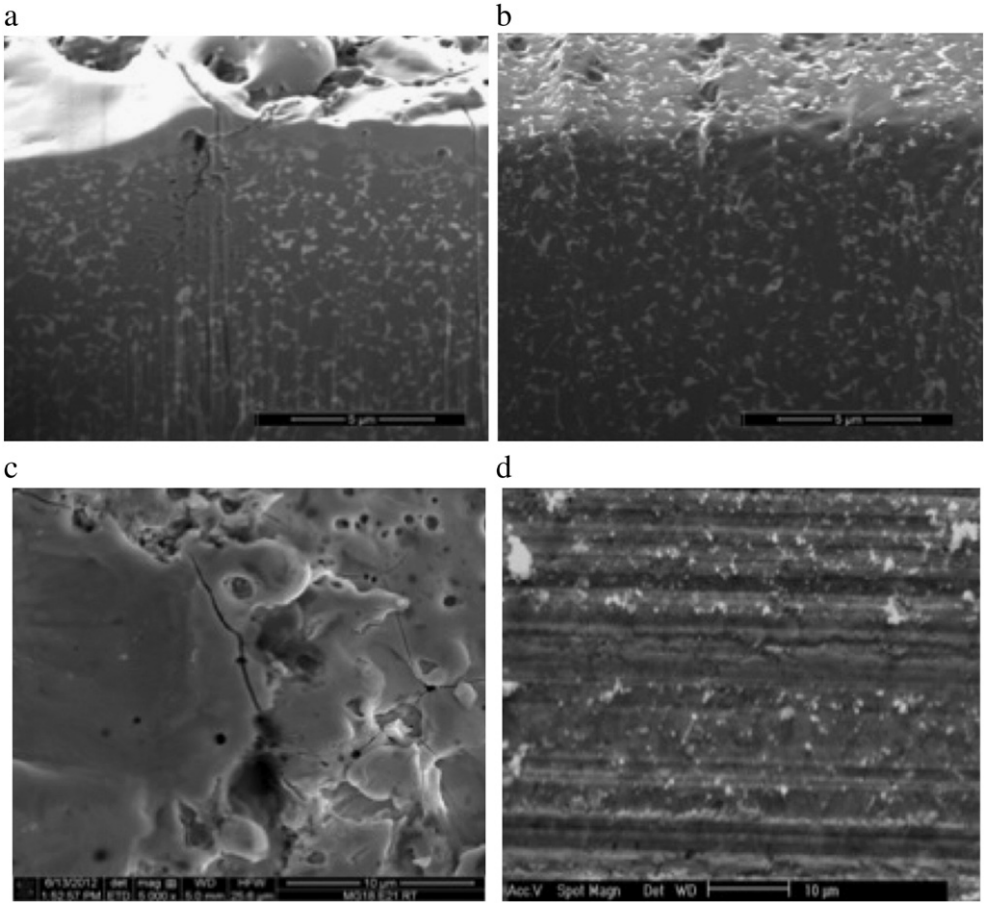

Fig. 2. FIB-SEM cross-section of the samples before the wear test: (a) wire-EDM sample (E21); (b) ground sample (G); (c) top surface of the E21 sample; and (d) top surface of the G sample.

as the reference surface finish condition and will be referred to as ' G', throughout the text.

The surface roughness of both the surface finish variants of E21 and G samples of cemented carbides was measured by means of surface profilometry (Somicronic® EMS Surfascan 3D, type SM3, needle type ST305), according to the ISO 4288 standard.

The resulting arithmetic mean roughness values (Ra) were 0.22 μm and 0.23 μm for the ground and wire-EDM'ed specimens, respectively. It is worth noting that the Ra roughness level of both materials and surface finishes is very similar to each other. Thus, the surface roughness effect can be neglected.

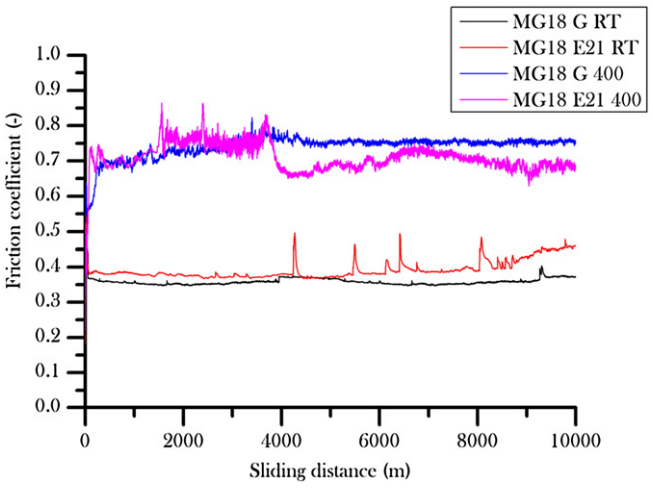

Fig. 3. Evolution of the friction coefficients with the sliding distance at 25 °C and 400 °C for the samples under study. (Normal load = 14 N; sliding velocity = 0.3 m/s).

Both the stress state and the bending strength of the WC10Co(Cr/V) bulk material ground and W-EDM, respectively were determined in a preceding research. Details of the experimental settings were published elsewhere [26]. The surface stresses, measured by X-ray diffraction using the d-sin$^2\psi$ method, indicated that the compressive stress state of the G sample raised to approximately 1.652 ± 0.106 GPa, owing to the mechanical impact of the grinding operation, in contrast with the stress state in the wire-EDM surfaces, for which tensile stresses were of the order of 537 ± 51 MPa.

Regarding the results on the flexural strength experiments, a value of 3508 ± 168 MPa was determined for the G sample, which is nearly 2.7 times greater than the value of 1327 ± 88 MPa found for the E21 sample, as a consequence of the presence of an important number of defects and flaws, which were produced during the W-EDM machining.

2.2. Wear tests

Systematic wear tests according to the ASTMG99-95a standard were carried out for assessing the influence of the surface finish on the friction and wear behavior of the WC-based cemented carbides. The tests were carried out at temperatures of 25 °C and 400 °C, respectively employing a pin on disk configuration, on a high-temperature tribometer (CSM, Switzerland) in atmospheric unlubricated conditions (60 ± 1% relative humidity). Pins of WC6Co(Cr/V) were used as static counterpart, with 6 mm diameter and surface roughness R_a and R_t values of 0.35 μm and 2.68 μm, respectively.

The wear experiments were performed under a normal force of 14 N, which produced a Hertzian maximum pressure of ~3 GPa. The

sliding speed was of 0.3 m/s. Such values were chosen in order to have similar conditions in relation to those employed during reciprocating tests, reported previously [16,17]. The duration of each test run was associated with a sliding distance (s) of 10 km.

Before the wear tests, both pin and plate specimens were cleaned ultrasonically in distilled water with a detergent solution (2% Tickopur R33, 60 °C, 15 min) and immersed in acetone. Subsequently, the samples were cleansed in cold distilled water and dried in a stream of air.

After the sliding tests, the worn surfaces were cleaned by pressurized air. The generated wear was quantified volumetrically by means of a surface topography scanning equipment (Somicronic® EMS Surfascan 3D SM3, needle type ST305). The morphological characterization of the surface conditions of the samples under study before and after wear testing was carried out using a scanning electron microscope (SEM, XL-30 FEG, FEI, Philips, Eindhoven, The Netherlands), equipped with an energy disperse X-ray spectrometer (EDAX-Dx-4i, Philips, Eindhoven, The Netherlands). However, the morphological characterization of the sample sub-surface before and after the wear test was carried out by a combined scanning electron microscopy (SEM) and focused ion beam (FIB) techniques (FEI Nova 600 Nanolab Dual-Beam FIB). The rectangular sectioning process consisted of a high ion current milling (20 nA) followed by a cleaning step of the obtained section (0.5 nA). Both processes were carried out with a voltage of 30 kV. Additionally, ion beam irradiation was applied as "etching" technique in order to clearly reveal the different zones through the cross section. When appropriate parameters and shorter exposure times were used (50 pA and 10 μs), ions irradiated the surface creating a smoothing phenomenon on it.

The mechanical behavior of both systems at 25 °C was assessed by carrying out analytical calculations of the stress field created by a circular sliding contact under a spherical indenter, using ELASTICA®, a commercial program. Therefore, by knowing the friction coefficient values, which were determined from the pin-on-disk tests carried out at room temperature, the sliding contact conditions were modeled for two different tangential forces for the G sample and the E21 sample, respectively.

The residual stresses at the surface, which were reported above for both the G and E21 samples, were also included in the calculations in order to see their influence on the variation of the principal stresses with the positive x-direction, which coincides with the direction of the application of the tangential force.

The calculations were performed for the G sample by considering the contact between the spherical indenter and the bulk material. However, for the E21 sample, the modeling was carried out considering the contact between the indenter and a system composed of 2 layers and a substrate, i.e. the recast layer, the HAZ layer and the bulk material. This consideration was done based on the results presented by Qu et al. [14], who showed that large variations both for the calculated hardness and modulus of elasticity were obtained in all three regions when carrying out the nanoindentation characterization of the surface layers of electrical discharge machined on WC–10Co. These authors, after a rigorous study coupled with SEM technique, determined that the hardness and E modulus values varied respectively between 7.6 to 19.7 GPa and 239 to 514 GPa for the bulk material, whereas for the HAZ such parameters varied between 15 GPa to 20.4 GPa and 323 GPa to 515 GPa, respectively. For the recast layer, the variation was between 5.6 GPa to 17.3 GPa and 189 GPa to 411 GPa, respectively. These variations were explained in terms of the presence of porosity, the soft cobalt matrix, cracks and other defects within these regions.

Therefore, for the effect of the calculation, average values of the E modulus of 292 GPa and 394 GPa for the recast and HAZ layers, respectively, were taken into account, as reported by Qu et al. [14].

3. Results and discussion

3.1. Sample morphology

FIB SEM images of the prepared cross-sections of the E21 and G samples are presented in Fig. 2a and b, respectively. Fig. 2a reveals the presence of the recast layer, exhibiting droplets and voids together with (sub)surface micro-cracks of considerable extension (more than 5 μm) and superficial cracks, distributed randomly on its surface, characteristics which are in agreement with the typical morphology of a W-EDM carbide found for this sample and reported in the literature.

EDS X-ray analysis carried out in order to identify the elements corresponding to the three zones of sample E21, i.e. the recast layer, HAZ and bulk, has indicated a similar composition for the bulk and the HAZ where C, W and Co are present, whereas the recast layer contained small amounts of Cu, Zn and O as additional elements. These results corroborate the findings reported earlier [26], which explain the presence of O and Cu as a consequence of the melting and oxidation of the wire during machining.

3.2. Friction and wear characteristics

The effect of fine wire-EDM on friction response of the E21 cemented carbides with respect to the G sample is illustrated in Fig. 3 for both 25 °C and 400 °C, respectively. The friction coefficient

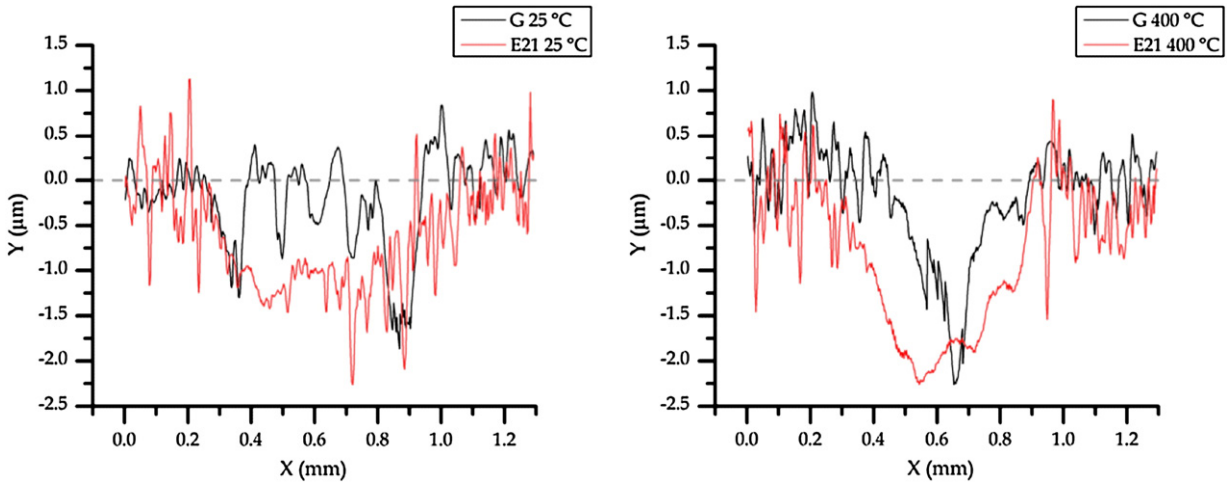

Fig. 4. Cross section profiles of the wear tracks of the samples at: 25 °C and 400 °C.

Table 3
Results from the wear tests.

Grade	Test temperature [°C]	WC–10wt.%Co(a)	
Surface finish		G	E21
Volume wear [$\times 10^{-2}$ mm^3]	25	1.8 ± 0.3	5.5 ± 0.8
	400	1.9 ± 0.3	6.5 ± 0.9
Specific wear rate	25	1.3 ± 0.2	4.0 ± 0.6
[$\times 10^{-7}$ mm^3/N.m]	400	1.3 ± 0.3	4.7 ± 0.7

that is reported below corresponds to an average of 3 experiments performed under identical conditions and with standard deviations of less than 10%.

At 25 °C, the variation of the friction coefficient for both samples with the sliding distance presents similar features, i.e. an increment during the first sliding meters, which corresponds to the running-in period, followed by a decrease in its value towards a steady state, which was achieved only by the G sample.

The average values of the friction coefficients were 0.36 ± 0.04 and 0.39 ± 0.06 for the ground and wire-EDM surface finishes, respectively. Moreover, it could be seen that, although the difference between the average friction coefficient values exhibited by both samples is insignificant at this temperature, the E21 sample could not reach the steady state even at high sliding distances due to the slow, but continuous removal of particles as a consequence of the presence of a considerable amount of cracks. The wire-EDM'ed sample randomly evidenced a sudden increase in the friction coefficient value up to 0.48 during the test. This difference in the friction level between wire-EDM'ed and the ground samples appears to increase slightly with increasing sliding distance.

The values of the friction coefficients between similar tribopairs of WC–10%Co reported in the literature for the tests carried out at room temperature are somewhat contradictory. Comparable average values for the friction coefficient of approximately 0.3 were reported recently for WC–Co samples produced by spark plasma sintering (SPS) [27]. The tests were carried out under dry conditions using a pin on plate tribometer by sliding a 6 mm WC–6wt.%Co pin against polished samples of WC–10%Co, at a constant linear speed of 0.10 m/s and with an applied normal load of 30 N. These test conditions led to a Hertzian maximum pressure of 3.45 GPa. Espinoza et al. [28], when tested WC–Co–C_3C_2–VC cemented carbides against WC–6%Co ball of 5 mm radius and a normal load of 40 N in dry sliding conditions at room temperature, obtained an average value of 0.35. This normal load produced a value of the Hertzian maximum pressure, P_{max}, in static conditions of 3.12 GPa, which is nearly equal to that calculated for the wear test conditions employed in the present research work (P_{max} = 3.10 GPa). Bonny et al. [29], carrying out reciprocating sliding experiments of similar tribopairs, with a pin of 4 mm radius and a load of 100 N, obtained an average friction coefficient of 0.4 for a P_{max} of 5.95 GPa. However, these results do not agree with those published by Casas et al. [23], who determined a value of the friction coefficient corresponding to the steady state equal to 1 at room temperature and in a pin-on-ring tribometer, where pins of WC–10%Co of 4 mm diameter were employed and the materials were tested at 0.5 m/s sliding velocity and 56 N normal load. The maximum pressure for the Hertzian contact was determined to be equal to 5.1 GPa.

As can be seen in Fig. 3, the friction coefficient becomes larger when the wear test is performed at 400 °C and all the events, which are mirrored by its variation with the sliding distance, constitute an indication of the wear mechanism, which takes place during the wear test.

It is well known that as the temperature increases, the mechanical properties of the WC–Co cermets decrease. It has been shown [30,31] that between 20 and 900 °C, the hardness of WC–6%Co and WC–10%Co alloys at all temperatures decreases with increasing the WC grain size, according to a Hall–Petch type relationship.

The increase in temperature will bring about a decrease in hardness for both individual phases (WC and binder) and, this decrease will be more accentuated (i.e. the value of the slope of the curve showing the dependence of hardness with the grain size) for the hard metal whose cobalt content is higher [30,31]. Therefore, although the increase in temperature will produce a drop in the hardness values of the tribopairs under study, the relative difference between their hardness values, which exists at room temperature, will still be maintained at higher temperatures. In these conditions, a more pronounced adhesion mechanism will take place and this will bring about an increase in the friction coefficient to an average value of more than two times higher at the temperature of 400 °C for the G sample, as compared to the value recorded at room temperature.

An average value of the friction coefficient of 0.75 ± 0.1 was determined and, again, this value is different to that of 0.6, which is the value reported previously by Casas et al. [23] for similar tribopairs tested at 400 °C. For the E21 sample a similar average value of the friction coefficient of 0.71 ± 0.8 was determined. Nevertheless, it could be noticed from the friction evolution curve that for the E21 sample all the individual values are higher than those corresponding

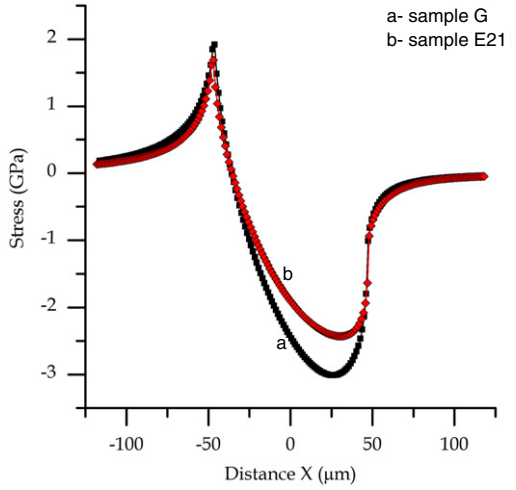

Fig. 5. Change of the σ_{xx} stress component with the distance for: (a) G sample (normal load = 14 N; μ = 0.36) and (b) E21 sample (normal load = 14 N; μ = 0.39).

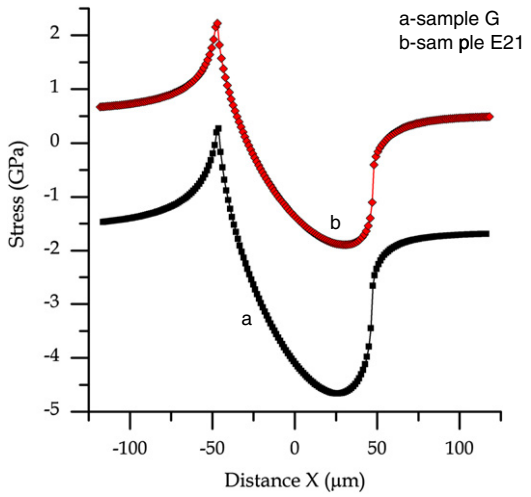

Fig. 6. Change of the σ_{xx} stress component with the distance for: (a) G sample frictional force = 5.04 N and compressive residual stresses = −1.65 GPa and (b) E21 sample frictional force = 5.46 N and the tensile residual stresses = 0.54 GPa.

Table 4
Young's modulus and mechanical properties of the tribosystems under study.

	Thickness (μm)	E modulus (GPa)	Poisson constant	TRS (GPa)	Residual stress (GPa)
Indenter WC–6Co pin ϕ = 6 mm	Infinite	609	0.29	3.780	
G sample bulk	Infinite	541	0.29		−1.652
E21 sample			0.29	1.327	+0.537
• Recast layer	4.92	292[a]			
• HAZ	7.16	394[a]			
• Bulk	Infinite	541			

[a] Reference [14].

to the G sample, up to a sliding distance of 3700 m. The variation of the friction coefficient is also characterized by sudden increases as a consequence of the wearing off of the main part of the weak recast layer, which led to a high amount of debris. After 3700 m of the sliding distance, the friction coefficient starts to drop slightly, showing a smaller value at the end of the test than the value of the friction coefficient corresponding to the steady state determined for the G sample.

3.3. Specific wear constant

Profilometry of the tracks was used to assess the amounts of material deposition and removal from the plate surface. Typical post-processed profiles of worn tracks on the plate at room and at 400 °C are displayed in Fig. 4.

The post-mortem assessment of the wear scar dimensions on the plate, i.e. volume, was measured using topographical scanning equipment (Hommel Somicronic® EMS Surfascan 3D, type SM3, stylus type ST305, Saint-André-de-Corcy, France). The area of the worn track was integrated from the 2D profile and further multiplied by the circular periphery with 7 mm radius.

The values of the specific wear rate for the G and E21 samples are indicated in Table 3.

As it could be observed, the W-EDM sample has a specific wear rate, which is approximately 3.1 times higher than that corresponding to the G sample at 25 °C. This behavior at room temperature could be explained by taking into consideration the results obtained from the analytical modeling of the contact stresses for these samples at 25 °C, explained below.

Table 5
Results from the analytical calculations indicating the values of the principal stresses, the maximum tensile stresses and von Mises stresses for the two conditions applied to the samples G and E21 (normal load 14 N).

Surface finish	1st case		2nd case	
	G[a]	E21[b]	G[a]	E21[b]
Normal load [N]	14	14	14	14
Friction coefficient	0.36	0.39	0.36	0.39
Friction force [N]	5.04	5.46	5.04	5.46
Residual stresses [GPa]	0	0	−1.65	0.54
Contact radius, a [μm]	46.52	47.24	46.52	47.24
Contact area [μm^2]	6800	7011	6800	7011
Mean contact pressure [GPa]	2.06	2.00	2.06	2.00
Maximum contact pressure [GPa]	3.1	3.0	3.1	3.0
Principal stress, σ_{xx} [GPa] at x = −a [μm], y = 0, z = 0	2.30	1.95	0.64	2.50
Principal stress, σ_{yy} [GPa] at x = −a [μm], y = 0, z = 0	−0.05	0.14	−0.06	0.14
Principal stress, σ_{yz} [GPa] at x = −a [μm], y = 0, z = 0	−0.00	−0.01	−0.01	−0.01
von Mises stress [GPa] at x = −46.17 [μm], y = 0, z = 0	2.30	1.95	0.70	2.50

[a] Ground.
[b] Wire-EDM E21.

3.4. Correlation between surface integrity, contact response and residual stresses

It is well known, that for an elastic tribocontact, the flat material experiences large compressive stresses. Within the contact circle, the applied load is distributed as a hemispherical compressive stress, while the maximum tensile stress is at the edge of the contact circle. However, the friction at the contact significantly modifies the stress field near the contact area and this will be even more affected by the sign of the residual stresses at the sample surface.

As indicated by Hamilton [32], with brittle materials the appearance of tensile stresses at the surface is far more important than the value of the yield parameter. In the present work, two cases were considered in the calculations. The first case (see Fig. 5) takes into account only the values of the normal and frictional forces for each sample. According to Hamilton [32], the σ_{xx} component of the stress state under these conditions is given by the following equations:

$$\sigma_{xx} = \frac{3P}{2\pi a^3}\left[\frac{(1-2\nu)\left(x^2-y^2\right)a^3}{3r^4}\right] + \frac{3\mu P}{2\pi a^3}\left[\frac{axM_0}{r^4} - x\phi\left(1+\frac{\nu}{4}\right)\right] \text{ if } |r| > |a| \quad (1a)$$

Otherwise:

$$\sigma_{xx} = \frac{3P}{2\pi a^3}\left\{\frac{1}{r^2}\left[\frac{\left(y^2-x^2\right)}{r^2}\left(F_1 - F_2\right)\right]\right\} - \frac{3\mu P}{2\pi a^3}\left[\frac{x\pi}{2}\left(\frac{\nu}{4}+1\right)\right] \quad (1b)$$

In the above equations:

$$r^2 = x^2 + y^2 \; ; \; M_0 = \left(r^2 - a^2\right)^{\frac{1}{2}} \; ; \; \phi = \tan^{-1}\left(\frac{a}{M}\right) \quad (2a)$$

where

$$M = \left(\frac{S+A}{2}\right) \; ; \; A = r^2 + z^2 - a^2 \; ; \; S = \left(A^2+4a^2z^2\right)^{\frac{1}{2}} \quad (2b)$$

also:

$$F_1 = \frac{(1-2\nu)}{3}F_0; F_0 = \left(a^2-r^2\right)^{1.5} - a^3 \text{ and } F_2 = \left(x^2+2\nu y^2\right)\left(a^2-r^2\right)^{\frac{1}{2}} \quad (2c)$$

x, y and z represent the axes of the coordinate system, P the normal load, a, the Hertzian contact radius, ν Poisson's ratio and μ the friction coefficient.

The curves shown in Fig. 5, corresponding to the G and E21 samples, respectively, describe the stress distribution as a function of the x direction according to Eqs. (1a) and (1b). In the particular case that y = z = 0 and x = −a, the maximum value of σ_{xx} is attained [32]:

$$\sigma_{xx}^{max} = \frac{3P}{2\pi a^2}\left[\frac{1-2\nu}{3} + \frac{4+\nu}{8}\pi\mu\right] \quad (3)$$

which occurs at the trailing edge of the contact (x = −a), whose trajectory is similar to the crack path.

For the second case, the residual stresses, which exist at the surface, were added to the value of σ_{xx} at the location x = −a, for each sample. Fig. 6 illustrates the results obtained for samples G and E21, respectively.

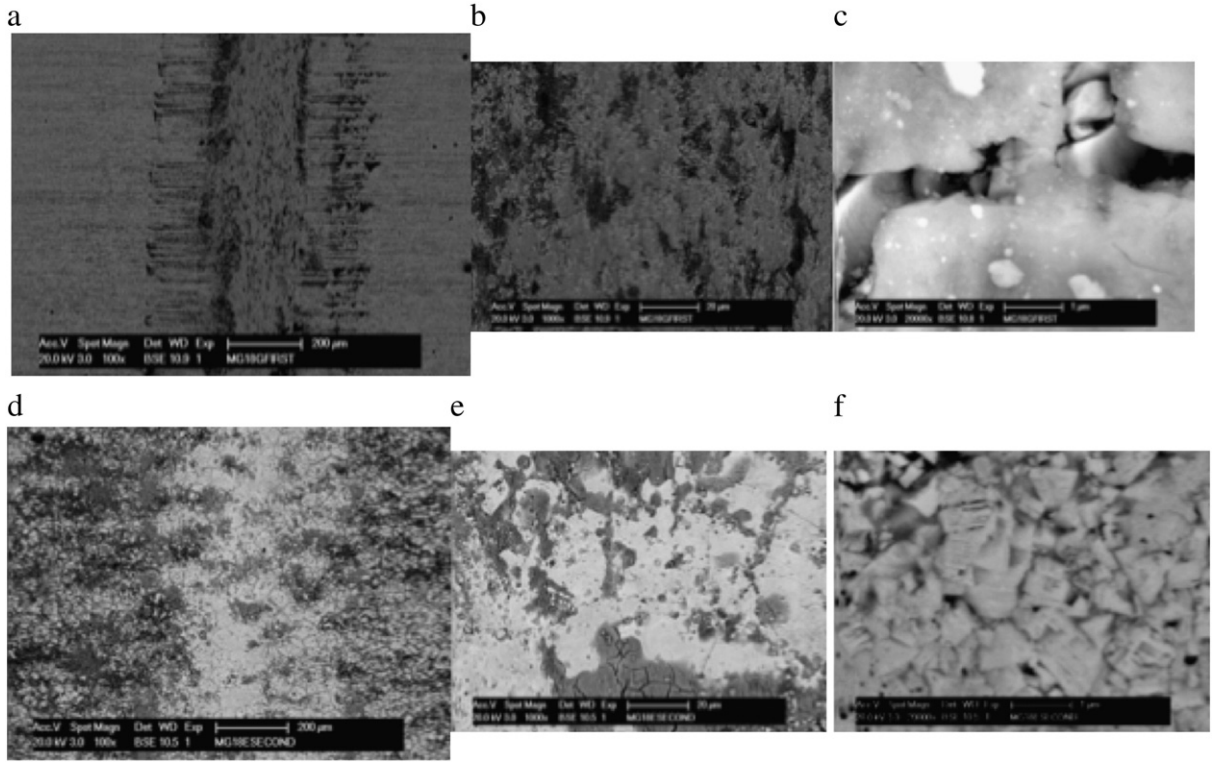

Fig. 7. SEM micrographs (BSE mode) of the samples G and E21: (a) wear track of the G sample; (b) detail of the micrograph presented in (a); (c) micrograph showing in detail the tribofilm formed over the wear track surface of the sample G; (d) wear track of the E21 sample; (e) detail of the micrograph presented in (a); and (f) micrograph showing the grain micro-fracture and grain pull-out in the wear track surface of the sample E21.

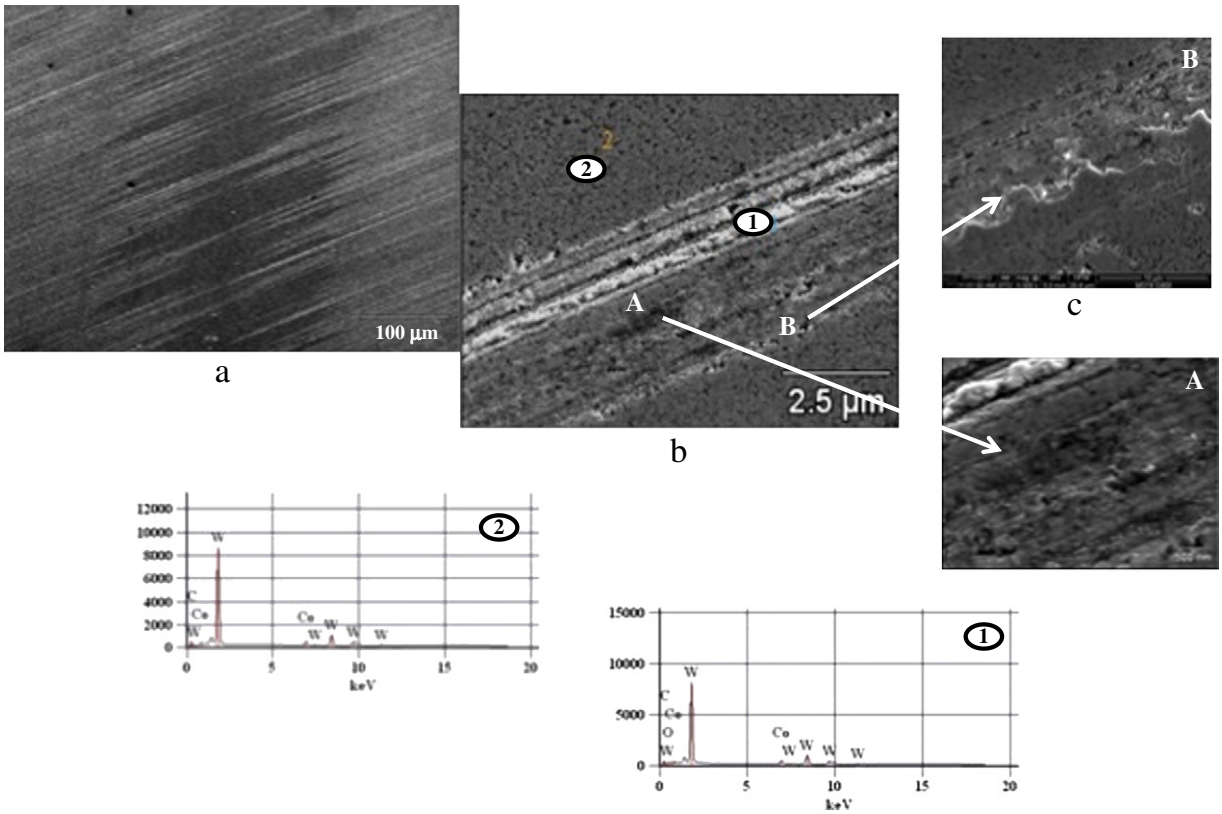

Fig. 8. (a) SEM of the G sample wear track at 400 °C; (b) detail of (a) and EDS analysis of the points 1 and 2 indicated in the micrograph; (c) detail of points A and B indicated in micrograph (b).

The data related to the mechanical properties taken into consideration for the calculations are presented in Table 4 and the results are indicated in Table 5.

It is well known that when the friction coefficient is equal to 0, i.e. under pure Hertzian static indentation conditions, one of the principal stresses at the surface is tensile near the edge of the contact and the stress distribution is symmetrical. As the friction coefficient rises, it can be seen that the σ_{xx} stress component is still the highest tensile stress, which acts in the plane of the surface and has almost the same value for both samples G and E21. This stress acts in the radial direction in the back edge of the contact and is the most likely point of failure, producing the well known ring cracks.

However, it can be seen from Fig. 6 that under sliding conditions the presence of tensile residual stresses at the surface of the E21 sample produces even a higher tensile stress whose value is approximately 4 times higher at the back edge contact than those corresponding to G sample, since the compressive surface stress layer after grinding decreases considerably the imposed frictional contact stress from 2.5 GPa to nearly 0.7 GPa.

Furthermore, it can be noticed that the sign σ_{xx} in front of the indenter is also different for the E21 and G samples during the contact, indicating compressive stresses in the case of the latter.

These findings suggest that, in this case, a better wear performance should be expected for the G sample and this behavior could be explained by taking into consideration the Linear Elastic Fracture Mechanics (LEFM) criterion that when the maximum tensile stress, σ_{xx}^{max} equals to or exceeds the values of K_{IC}, the cracks will propagate on the surface of the material in a catastrophic manner:

$$\beta\sigma_{xx}^{max}\sqrt{\pi d} \geq k_{IC} \quad (4)$$

K_{IC}	the plane strain fracture toughness
σ_{xx}^{max}	the maximum tensile stress at the crack tip
β	geometrical factor
d	length of the critical flaw size.

If the values of the maximum tensile stresses determined in Table 5 are substituted in the above equation and considering that the value of K_{IC} for both samples is equal, it shows that the ratio $\sigma_{xx}^{max}{}_{G\ sample}/\sigma_{xx}^{max}{}_{E21\ sample}$ is inversely proportional to the ratio of their critical flaw size $d_{E21\ sample}/d_{G\ sample} = 0.06$, indicating once more the weakness of the E21 system.

It is interesting to observe from Table 2 that the wear rate coefficient, k, at 400 °C is almost the same as that reported for the room temperature test for the sample G and just somewhat higher (approximately 15%) than the value corresponding to the E21 sample, indicating that apparently the test temperature does not have an important effect on the wear rate, but, as we shall see below, on the wear mechanism between tribopairs.

Similar analytical calculations for the sliding contact were not performed at 400 °C, since the elastic properties of hard metal alloys at higher temperature are seldom found in the literature.

However, at this point, it is important to mention what are the main changes related to the increase in temperature. It is well known, that the mechanical properties and chemical stability of cemented carbides can strongly be affected by the increase in temperature. Mechanical properties such as transverse rupture strength (TRS), yield stress, σ_s, and strain at fracture δ were reported in detail by Yu and co-workers [33] for cemented carbides with micron and submicron sizes, different Co contents ranging from 6 to 15% and for temperatures varying between 20 and 1000 °C. It was shown, for example, that both the fracture stress (TRS) and Young's modulus decrease with increasing temperature slowly up to 600 °C, but all these alloys will display ductility only at temperatures higher than 600 °C, when they will exhibit a considerable drop in their values. These authors have reported that for a similar composition and morphological characteristics of carbides as those considered in the present study, the relationship between (HV/σ_s) will increase from 3.04 at 25 °C to nearly 6.5 at 400 °C and plastic deformation will be able to take place only in the Co binder, which will lead to very low strain at fracture.

Therefore, a very important factor that should be taken into consideration in order to explain the wear behavior at 400 °C is the fact that, as the test temperature increases, the level of residual stresses introduced as a consequence of the fabrication and the sample preparation process will decrease slightly. As quoted in the literature [23,34], for example, the decrease in the tensile residual stresses will eventually reduce the possibility of the propagation of the existing cracks between the interface cobalt-carbide, which in turn will promote an increase in the fracture energy, hindering the detachment of material particles and enhancing the adhesion mechanism between tribopairs.

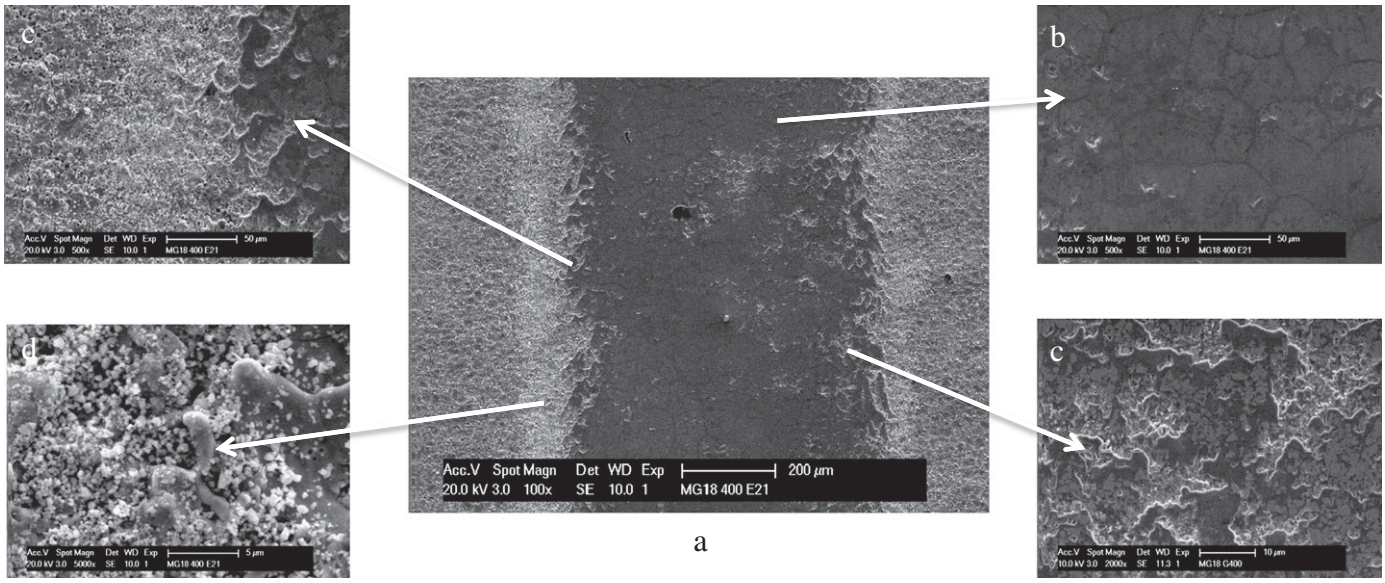

Fig. 9. (a) SEM of the E21 sample wear track at 400 °C; (b) detail of (a) in the center of the wear track showing the high amount of cracks; (c) details of the wear track near the border indicating some adhesion mechanism and (d) the high amount of debris produced during the test, near the border of the wear track.

3.5. SEM and wear mechanism

The SEM micrographs corresponding to the worn surfaces are presented in Fig. 7 for both the G and E21 samples at room temperature. It can be seen that, in the case of the G sample, a tribofilm is formed which covers the contact surface almost completely in the center, leaving some WC grains to be seen through it. The SEM micrograph (Fig. 7c), in backscattering mode, indicates that the film is made of a mechanical mixture of sub-micron particles of WC, which were produced as debris due to the abrasion mechanism that takes place when the pin is slid against the surface and the existing Co binder. It is well known that the wear products could in turn cause scratching and extraction of binder between carbide grains [35].

Cobalt, at a temperature less than 500 °C, is very brittle and under load, fracture can occur starting at WC/WC grain boundaries. Then, the crack travels through the binder and grain boundaries by the so-called multi-ligament cracking mechanism [36], when the cobalt forming the ligaments is free from constraints and could be deformed and squeezed out, leaving the WC grain without the protection.

However, in case of the E21 sample, the contact between the pin and the sample is modified by the presence of the recast layer and the tribo-compatibility, that characterized the sample G, is no longer existent. As it was mentioned previously, high amounts of debris are eliminated from the contact and only small quantities of them were retained over the wear track surface. Debris formation is assisted by the presence of considerable amount of cracks (see Fig. 2), which will propagate in the plane where the highest tensile stresses, σ_{xx}^{max}, calculated in Table 5, act perpendicularly.

Fig. 8 shows the typical morphology of the wear track after the test carried out on the G sample at 400 °C. It can be seen that the amount of oxygen, as indicated by the EDS analysis performed in point 2, is almost negligible. However, the %O is higher for point 1, which shows the presence of some debris retained in the wear track that have been oxidized due to their contact with air and higher local temperature. Plastic deformation is also present in A, which corroborates the deformation behavior classification of WC–Co as function of temperature, carried out by Buss [36]. This author indicated that, under this temperature conditions, i.e. 400 °C, the mechanical behavior of the WC–Co system corresponds to a so called "second domain of deformation" that is characterized by the plastic deformation of the binder, with no considerable plastic deformation of WC. Some detachment of WC grains could also be observed in B.

Fig. 9 corresponds to the morphology of the E21 sample tested at 400 °C. It could be seen that in this case a considerable amount of debris particles are mainly located in the outer extensions of the wear track, whereas the center of the wear track presents a smoother surface as compared to the initial morphology of the E21 sample, which exhibited large amount of micro-cracks and porosities.

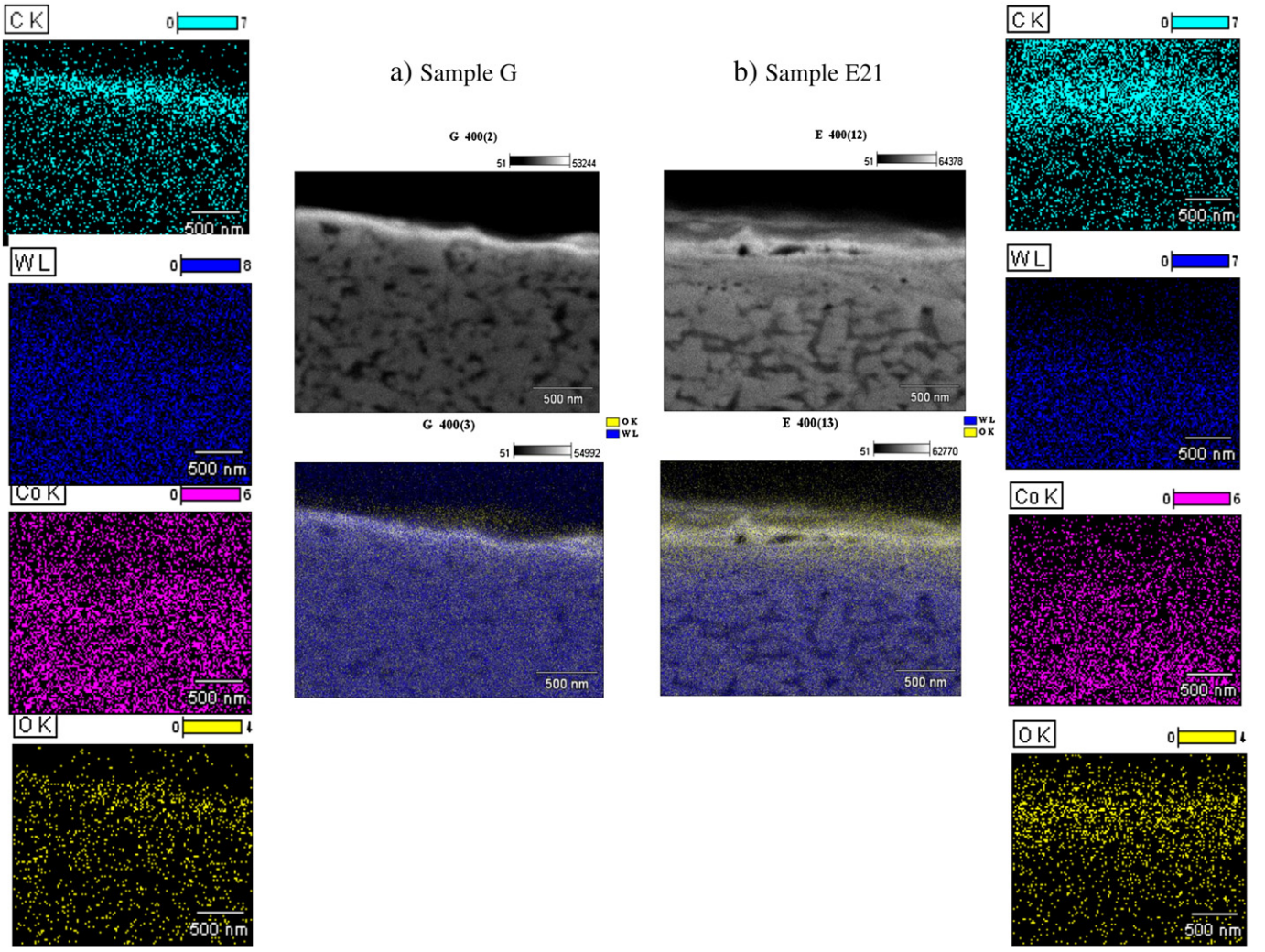

Fig. 10. (a) SEM micrograph and element X-ray mapping of the worn G sample tested at 400 °C indicating the distribution of C, W, Co and O; (b) SEM micrograph and element X-ray mapping of the worn E21 sample tested at 400 °C indicating the distribution of C, W, Co and O.

It was mentioned previously that at the end of the wear test carried out at 400 °C, a smaller value for the friction coefficient was found for the sample E21. The existence of a higher amount of oxygen in the recast layer as compared to the G sample, probably, could explain this behavior. Oxygen mapping carried out during the SEM analysis on metallographically prepared cross-sections of both wire-EDM and ground samples corroborates these findings (see Fig. 10). Another important feature found from the SEM mapping of the cross-section of the wear track of the samples was related to the distribution of C and Co. A higher amount of C is observed for both samples near the surface, as compared to the bulk. Also, the amount of Co is higher in the G sample as compared to the E21 sample. However, it has to be remembered that Co depletion for the E21 sample occurs as a consequence of W-EDM processing [26].

It is interesting to observe from Fig. 11 that even after 10 km of the sliding distance, the typical morphology of the recast layer is still present, having a thickness of approximately 500 nm and showing a polished surface with its characteristic features (see Fig. 11b).

The specific wear rate of the pins was not determined due to the presence of adhered material from the plate. However, to better understand how the worn surfaces on the balls evolved, EDS was employed to carry out a chemical analysis of their surfaces. The key difference in alloy content between the pin and E21 plate material is that that the latter had in its composition a small amount of Cu, coming from the W-EDM processing. This element will be absent from the pin material. While it is not a quantitative technique, the presence or absence of Cu peaks in the EDS spectra can be used to detect whether the E21 plate material has been transferred to the pin. The same procedure was employed for the G sample and its corresponding pin by carrying out Co analysis outside the wear scar and inside it. An increase of the %Co inside the wear scar will be an evidence of material transfer from the plate to the pin, since the Co content is higher in the plate.

Fig. 12 shows the representative SEM micrographs of the wear scars produced on the pins corresponding to all the wear test conditions employed in this research and Table 6 shows the results from the semi-quantitative EDS analysis carried out for each point indicated in the respective micrograph.

Another interesting aspect is the variation of the %O in this table for each pin wear scar, as compared to the respective base material.

4. Conclusions

The friction and wear responses of two WC–10%Co(Cr/V) cemented carbides were evaluated at 25 °C and 400 °C, by carrying out sliding wear tests against WC–6%Co(Cr/V) balls in a high temperature tribometer. In this way, it was possible to determine the influence of the surface finish produced by the machining processes.

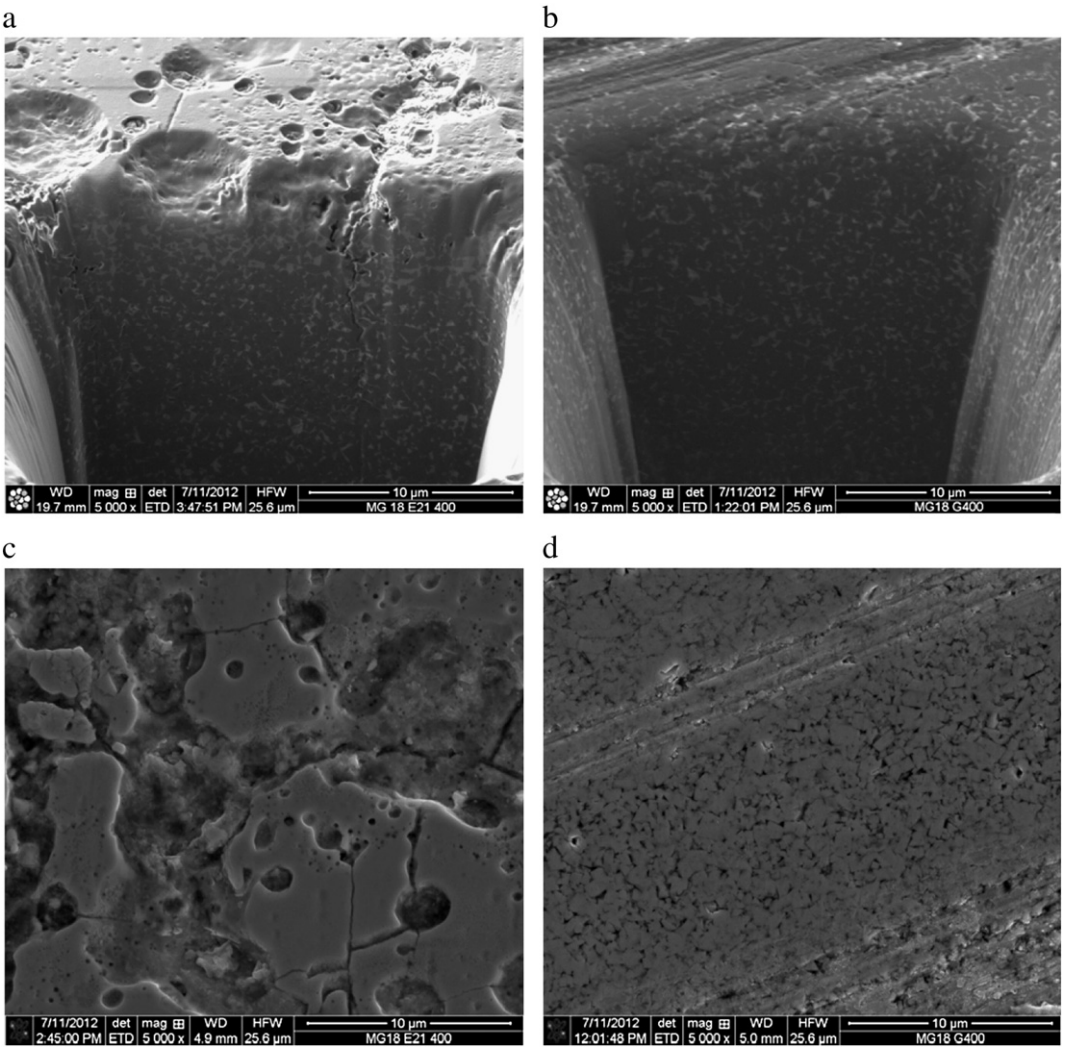

Fig. 11. FIB-SEM cross-section of the samples after the wear test at 400 °C: (a) wire-EDM sample (E21); (b) ground sample (G); and top surface of: (c) E21 sample and (d) G sample.

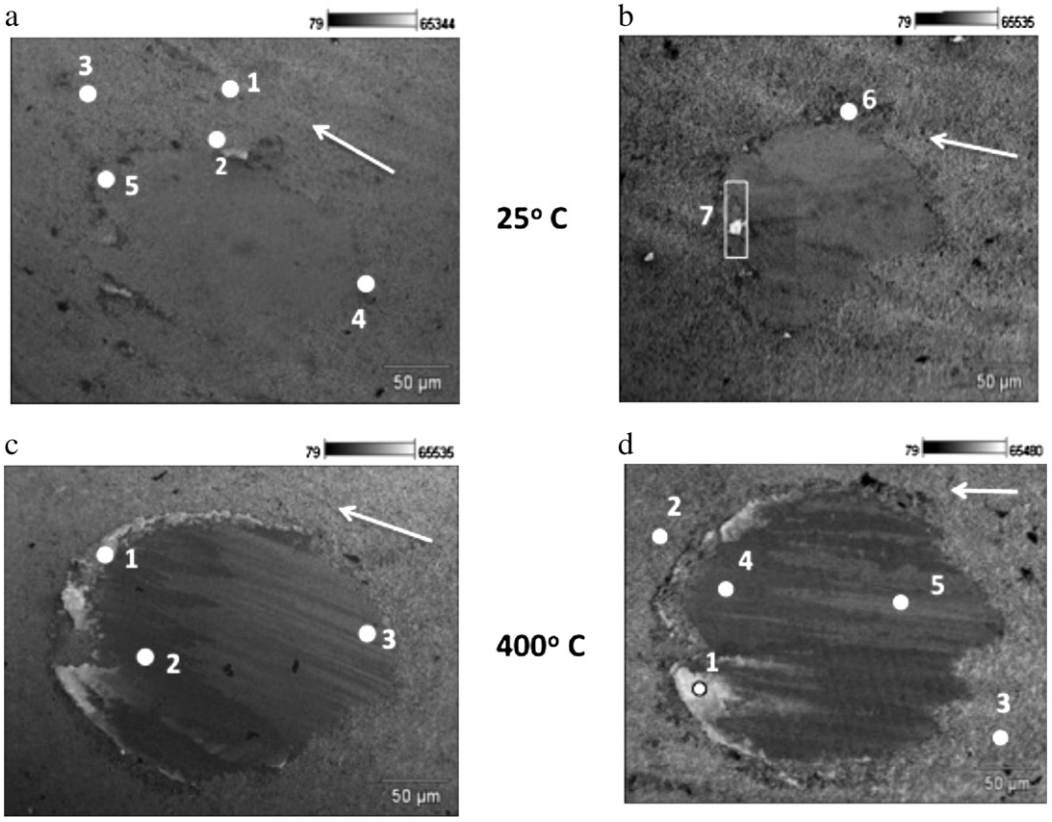

Fig. 12. (a) Morphology of the WC6Co(Cr/V) pin surface after sliding against G sample at 25 °C; (b) morphology of the WC6Co(Cr/V) pin surface after sliding against E21 sample at 25 °C; (c) morphology of the WC6Co(Cr/V) pin surface after sliding against G sample at 400 °C; (d) morphology of the WC6Co(Cr/V) pin surface after sliding against E21 sample at 400 °C.

The results have shown that:

- At a temperature of 25 °C the average values of the friction coefficients were 0.36 ± 0.04 and 0.39 ± 0.06 for the ground (G sample) and wire-EDM (E21 sample) surface finishes, respectively. The specific wear rate for the E21 sample is approximately 3.1 times higher than that corresponding to G sample, as a consequence of the microstructural changes that took place during the surface finish process. This behavior was explained by taking into consideration the results obtained from the analytical modeling of the stress field created by a circular sliding contact, under a spherical indenter, where the values of the residual stresses inherent to each sample were considered. For the E21 sample, the modeling was carried out considering the contact between the indenter and a system composed of 2 layers (recast layer and HAZ layer) and the substrate, due to the large variation in their elastic properties. In this case, it was shown that the presence of tensile residual stresses at the surface of the E21 sample increases the value of σ_{xx}^{max}, which is approximately 4 times higher than that corresponding to G sample. For the latter, the compressive surface stress layer decreases the imposed frictional contact stress, from 2.5 GPa to nearly 0.7 GPa. Also, it was found that, for the G sample, the stresses in front of the indenter are of a compressive nature.
- By means of Linear Elastic Fracture Mechanics (LEFM), it has been shown that the critical flaw size for the E21 sample is only 0.06 times that of the critical flaw size of the G sample, which explains its poor tribological performance.
- At 400 °C, an increase in the friction coefficients takes place up to values of 0.75 ± 0.1 and 0.71 ± 0.8, for the ground and wire-EDM surface finishes, respectively. For the G sample a more pronounced adhesion mechanism takes place and this brings about an increase in the friction coefficient to an average value of more than two times, as compared to the value recorded at room temperature. However, for the wire-EDM sample this increase was more linked to a marked abrasive wear mechanism due to the presence of the weak recast layer, which led to a high amount of debris.
- The wear rates for both samples at 400 °C are similar to those obtained at 25 °C, which indicates that apparently the test temperature does not have an important effect on this parameter. However, an important factor that should be taken into consideration in order to explain the wear behavior of the E21 sample at 400 °C is the fact that, as the test temperature increases, the level of tensile residual stresses introduced as consequence of machining decreases slightly. This phenomenon will, eventually, reduce the possibility of the propagation of the existing cracks.
- From the morphological features observed from the SEM-EDS analysis, it was shown that after 10 km sliding distance, the E21 sample

Table 6
EDS analysis of the points indicated in (a) and (b) for the samples at 25 °C; (c) and (d) for the samples at 400 °C.

Figure	Sample/ball at 25 °C	C–K	O–K	Cr–K	Co–K	Cu–K	W–L
12 a	Pt1	27.92	4.64	0.22	4.39		61.95
	Pt2	25.46	2.13	0.36	2.33		69.72
	Pt3	27.76	0.39	0.19	1.9		69.77
	Pt4	31.61			1.13		67.05
	Pt5	29.71	5.97		2.4		61.92
12 b	Pt6	22.86	2.73	0.32	3.24	0.56	70.28
	Pt7	29.38	8.41	0.26	3.2	1.19	57.48
Figure	Sample/ball at 400 °C	C–K	O–K	Cr–K	Co–K	Cu–K	W–L
12 c	Pt1	30.47	13.21	0.04	2.98		53.3
	Pt2	21.41	10.96	0.35	4.5		62.78
	Pt3	38.08		0.37	3.25		58.3
12 d	Pt1	22.26	9.33	0.3	5.24	0.28	62.59
	Pt2	30.58	3.38	0.25	2.06		63.54
	Pt3	34.89	3.42	0.19	1.95		59.54
	Pt4	19.4	2.71	0.46	4.67	0.04	72.46
	Pt5	27.86	8.43	0.38	2.72		60.61

still maintains at its surface the recast layer of about 500 nm, with an appreciable amount of oxygen, i.e. a more lubricious film, which explains its satisfactory performance, despite the presence of cracks.

Acknowledgments

This investigation was supported by the Fund for Scientific Research Flanders (FWO, grant no. G.0539.08) and by the Flemish Institute for the promotion of Innovation by Science and Technology in Industry (IWT, grant no. GBOU-IWT-010071-SPARK). Research was performed within a cooperative effort among Ghent University (UGent) and the Catholic University of Leuven (K.U. Leuven). The authors gratefully acknowledge the involved research partners for all assistance, facilities, scientific contributions and stimulating collaboration. Professor Staia gratefully acknowledges the financial support received from Ghent University (BOF).

References

[1] Gadalla AM, Tsai W. Electrical plate charge machining of tungsten carbide-cobalt composites. J Am Ceram Soc 1989;72(8):1396–401.
[2] Puertas I, Luis CJ, Alvarez L. Analysis of the influence of EDM parameters on surface quality, MRR and EW of WC–Co. J Mater Process Technol 2004;153–154: 1026–32.
[3] Yu Z-B, Jun T, Kunieda M. Dry electrical plate charge machining of cemented carbide. J Mater Process Technol 2004;149(1–3):353–7.
[4] Lauwers B, Liu W, Eeraerts W. Influence of the composition of WC-based cermets on the manufacturability by wire-EDM. Trans NAMRI/SME 2004;32:407–14.
[5] Mahdavinejad RA, Mahdavinejad A. ED machining of WC–Co.J Mater Process Technol 2005;162–163:637–43 [(Spec. Iss.)].
[6] Lenz E, Katz E, König W, Wertheim R. Cracking behavior of sintered carbides during EDM. Ann CIRP 1975;24(1):109–14.
[7] Lee HT, Tai TY. Relationship between EDM parameters and surface crack formation. J Mater Process Technol 2003;142(3):678–83.
[8] Llanes L, Casas B, Idanez E, Marsal M, Anglada M. Surface integrity effects on the fracture resistance of electrical-discharge machined WC–Co cemented carbides. J Am Ceram Soc 2004;87(9):1687–93.
[9] Lee SH, Li X. Study of the surface integrity of the machined workpiece in the EDM of tungsten carbide. J Mater Process Technol 2003;139(1–3):315–21.
[10] Khan AA, Ali MBt Mohd, Shaffiar NBt Mohd. Relationship of surface roughness with current and voltage during wire EDM. J Appl Sci 2006;6(10):2317–20.
[11] Lin Y-C, Hwang L-R, Cheng C-H, Su P-L. Effects of electrical discharge energy on machining performance and bending strength of cemented tungsten carbides. J Mater Process Technol 2008;206(1–3):491–9.
[12] Jiang D, Anné G, Vleugels J, Vanmeensel K, Eeraerts W, Liu W, et al. Residual stress in hard metals caused by grinding and EDM machining and its influence on flexural strength. Proc. 16th Int. Plansee Seminar (Reutte, Austria)Powder Metallurgical High Performance Materials, vol 2; 20051075–85.
[13] Majid MA, Musa S. Impact and transverse rupture strength of electrically discharged machined die materials. Int J Join Mater 1998;10(3–4):92–7.
[14] Qu J, Riester L, Shih AJ, Scattergood RO, Lara-Curzio E, Watkins TR. Nanoindentation characterization of surface layers of electrical discharge machined WC–Co. Mater Sci Eng A 2003;344(1–2):125–31.
[15] Bonny K, De Baets P, Vleugels J, Van der Biest O, Lauwers B, Liu W. EDM machinability and dry sliding friction of WC–Co cemented carbides. Int J of Manuf Res 2009;4(4):375–94.
[16] Llanes L, Idanez E, Martinez E, Casas B, Esteve J. Influence of electrical plate charge machining on the sliding contact response of cemented carbides. Int J Refract Metals Hard Mater 2001;19(1):35–40.
[17] Ishikawa K, Iwabuchi A, Shimizu T. Influence of EDM on the wear characteristics of WC–Co cemented carbide. J Jpn Soc Tribologis 2003;48(11):928–35.
[18] Bonny K, De Baets P, Ost W, Vleugels J, Huang S, Lauwers B, et al. Influence of electrical plate charge machining on the reciprocating sliding wear response of WC–Co cemented carbides. Wear 2009;266(1–2):84–95.
[19] Bonny K, De Baets P, Ost W, Huang S, Vleugels J, Liu W, et al. Influence of electrical plate charge machining on the reciprocating sliding friction and wear response of WC–Co cemented carbides. Int J Refract Metals Hard Mater 2009;27(2):350–9.
[20] Bonny K, De Baets P, Quintelier J, Vleugels J, Jiang D, Van der Biest O, et al. Surface finishing: impact on tribological characteristics of WC–Co hardmetals. Tribol Int 2009. http://dx.doi.org/10.1016/j.triboint.2009.04.029.
[21] Perez Delgado Y, Bonny K, De Baets P, Neis PD, Malek O, Vleugels J, Lauwers B. Impact of wire-EDM on dry sliding friction and wear of WC-based and ZrO_2-based composite.Wear July 29 2011;271:1951–61 [Issues 9–10].
[22] Jianxin D, Hui Z, Ze W, Yunsong L, Jun Z. Int. Journal of Friction and wear behaviors of WC/Co cemented carbide tool materials with different WC grain sizes at temperatures up to 600 °C. Int J Refract Metals Hard Mater 2012;31:196–204.
[23] Casas B, Cardellach M, Alcalá J, Llanes y L. Influencia de la temperatura sobre la resistencia al desgaste de pares idénticos de WC–Co, VIII Congreso Nacional de Propiedades Mecánicas de Sólidos. Gandia 2002:571–8.
[24] Shi X, Yang H, Shao G, Duan X, Wang S. Oxidation of ultrafine-cemented carbide prepared from nanocrystalline WC–10Co composite powder. Ceram Int 2008;34: 2043–9.
[25] Bonny K, De Baets P, Vleugels J, Huang S, Van der Biest O, Lauwers B. Impact of Cr3C2/VC addition on the dry sliding friction and wear response of WC–Co cemented carbides. Wear 2009;267:1642–52.
[26] Jiang D, Anné G, Vleugels J, Vanmeensel K, Eeraerts W, Liu W, et al. Residual stresses in hardmetals caused by grinding and EDM machining and their influence on the flexural strength.In: Kneringer G, Rödhammer P, Wildner H, editors. Powder metallurgical high performance materials. Reutte, Austria: Plansee; 2005. p. 1075–85 [16th International Plansee Seminar].
[27] Picas JA, Xiong Y, Punset M, Ajdelsztajn L, Forn A, Schoenung JM. Microstructure and wear resistance of WC–Co by three consolidation processing techniques. Int J Refract Metals Hard Mater 2009;27:344–9.
[28] Espinoza L, Bonache V, Salvador MD. Friction and wear behavior of WC–Co–C3C2–VC cemented carbides obtained from nanocrystalline mixture. Wear 2011;272:62–8.
[29] Bonny K, de Baets P, Perez Y, Vleugels J, Lawers B. Friction and wear characteristics of WC–Co cemented carbides in dry reciprocating sliding contact. Wear 2010:1504–17.
[30] Milman YuV, Luyckx S, Northrop IT. Influence of temperature, grain size and cobalt content on the hardness of WC–Co alloys. Int J Refract Metals Hard Mater 1999;17:39–44.
[31] Milman YuV, Chugunova S, Goncharuck V, Luyckx S, Northrop IT. Low and high temperature hardness of WC–6 wt%Co alloys. J Refract Met Hard Mater 1997;15:97–101.
[32] Hamilton GM. Explicit equation for the stresses beneath a sliding spherical contact. Proc Inst Mech Eng 1983;197C.
[33] Milman YuV, Luyckx S, Goncharuck VA, Northrop JT. Results from bending tests on submicron and micron WC–Co grades at elevated temperatures. Int J Refract Metals Hard Mater 2002;20:71–9.
[34] Seol K, Krawitz AD. Anisotropic residual stress relaxation in cemented carbide. Mater Sci Eng A July 1990:1–5.
[35] Larsen-Basse J. Extrusion in sliding wear of WC–Co alloys. Wear 1985;105:247–56.
[36] Buss K. Thèse No 3095 (2004) École Polytechnique Fédérale de Lausanne, Faculté Sciences de Base, Institut de Physique de la Matière Complexe, Section de Physique, Grade de Docteur en Sciences; 2004.